nanomaterials

MDPI

Article

Low Reflection and Low Surface Recombination Rate Nano-Needle Texture Formed by Two-Step Etching for Solar Cells

Chia-Hsun Hsu [1], Shih-Mao Liu [2], Shui-Yang Lien [1,3,*], Xiao-Ying Zhang [1], Yun-Shao Cho [3,4], Yan-Hua Huang [5], Sam Zhang [6], Song-Yan Chen [7] and Wen-Zhang Zhu [1]

1 School of Opto-Electronic and Communication Engineering, Xiamen University of Technology, Xiamen 361024, China; chhsu@xmut.edu.cn (C.-H.H.); xyzhang@xmut.edu.cn (X.-Y.Z.); wzzhu@xmut.edu.cn (W.-Z.Z.)
2 Mechanical and Automation Engineering, Da-Yeh University, Changhua 51591, Taiwan; v0011009@gmail.com
3 Department of Materials Science and Engineering, Da-Yeh University, Changhua 51591, Taiwan; yunshaojhuo@gmail.com
4 Industry-University Center, Da-Yeh University, Changhua 51591, Taiwan
5 Chengyi University College, Jimei University, Xiamen 361021, China; anncy@jmu.edu.cn
6 Faculty of Materials and Energy, Southwest University, Chongqing 400715, China; SamZhang@swu.edu.cn
7 Department of Physics, OSED, Xiamen University, Xiamen 361005, China; sychen@xmu.edu.cn
* Correspondence: sylien@xmut.edu.cn

Received: 25 August 2019; Accepted: 25 September 2019; Published: 29 September 2019

Abstract: In this study, needle-like and pyramidal hybrid black silicon structures were prepared by performing metal-assisted chemical etching (MACE) on alkaline-etched silicon wafers. Effects of the MACE time on properties of the black silicon wafers were investigated. The experimental results showed that a minimal reflectance of 4.6% can be achieved at the MACE time of 9 min. The height of the nanostructures is below 500 nm, unlike the height of micrometers needed to reach the same level of reflectance for the black silicon on planar wafers. A stacked layer of silicon nitride (SiN_x) grown by inductively-coupled plasma chemical vapor deposition (ICPCVD) and aluminum oxide (Al_2O_3) by spatial atomic layer deposition was deposited on the black silicon wafers for passivation and antireflection. The 3 min MACE etched black silicon wafer with a nanostructure height of less than 300 nm passivated by the SiN_x/Al_2O_3 layer showed a low surface recombination rate of 43.6 cm/s. Further optimizing the thickness of ICPCVD-SiN_x layer led to a reflectance of 1.4%. The hybrid black silicon with a small nanostructure size, low reflectance, and low surface recombination rate demonstrates great potential for applications in optoelectronic devices.

Keywords: black silicon; passivation; metal-assisted chemical etching

1. Introduction

Silicon reflects a significant amount of incident light on its surface because of its high refractive index of about 3 to 4 in the visible wavelength region. The most common way to reduce the reflection is to texture the silicon surface by iso-etching, which produces micron-scale pyramids on the surface. A dielectric layer is deposited to further reduce the reflection based on the quarter-wavelength design and is therefore optimized only for a given wavelength [1]. Another way is to make nanostructures on a silicon surface (known as black Si [2,3]). A broadband antireflection at a wider acceptance angle than single or multilayer antireflective coatings can be achieved [4–8]. Black silicon can be prepared using reactive ion etching [9], laser–chemical [4,10], electrochemical [5], or metal-assisted chemical etching

(MACE) [11–14]. Some of the techniques produce regular nanostructures, but random textures can reduce reflectance equally well [15]. The MACE process leads to random textures. The metal source of the MACE process can be gold, silver nanoparticles mixed with hydrogen fluorine (HF) and hydrogen peroxide (H_2O_2) [6,7]. Due to the sharp nanostructures, the incident light experiences a varying refractive index as a composition of the silicon and the surrounding materials [5,16]. The fraction of the silicon increases when the light goes deeper inside the nanostructures.

Although black silicon has the advantage of low surface reflection, its large surface area leads to a large recombination rate. Long nanostructures with a small diameter lead to very low reflectance, but this does not improve the solar cell performance. Traditional MACE etching for solar cell applications is usually performed on planar wafers, which have high reflectance of about 30–40% in wavelengths of 400–1000 nm. In order to obtain sufficiently low reflectance, the etching depth needs to be deep, and thus, sharp, long nanostructures are produced. These structures increase the difficulties of the doping process and passivation of silicon surface. The emitter region becomes deeper with increasing the nanowire length, and photogenerated carriers at the tip of these nanostructures recombine before being collected at the junction [17]. Although black silicon demonstrates excellent optical properties, simultaneously achieving low reflectance and low surface recombination is getting more desirable and challenging [18].

In this study, a two-step etching process was performed, and it was able to give a low reflectance when the height of the nanostructures is less than 500 nm. The first step was the alkaline etching resulting in a pyramidal surface, and the second step was the MACE that creates needles on the pyramids of the alkaline-etched wafers. Compared to long, sharp nanowires produced by traditional MACE on planar wafers, the small sized nanostructures in turn mean a smaller amount of increase in surface area, and passivation will be relatively easier. In addition, the nanostructures can also be fabricated at a large scale. The MACE time was varied to produce different sizes of the nanostructures. The black silicon was passivated by aluminum oxide and silicon nitride by spatial atomic layer deposition (ALD) and plasma enhanced chemical vapor deposition (PECVD), respectively. The reflectance and the passivation quality of the black silicon wafers are presented and discussed. Low reflectance and high passivation on silicon wafers with small-sized nanostructures can be achieved.

2. Materials and Methods

Boron-doped crystalline silicon wafers with a thickness of 200 μm and a resistivity of 1 Ω-cm were used as substrates. The conventional MACE process was usually performed on planar wafers as shown in Figure 1a–c. When the Ag^+ ions were in contact with the silicon surface, they reduced to Ag particles and ejected holes into silicon, catalyzing local silicon oxidation beneath the Ag particles. The silicon oxidation was then dissolved by HF. The MACE process can be expressed by:

$$Ag^+ \rightarrow Ag + h^+, \quad (1)$$

$$Si + 2H_2O + 4h^+ \rightarrow SiO_2 + 4H^+, \quad (2)$$

$$SiO_2 + HF \rightarrow H_2SiF_6 + H_2O \quad (3)$$

where h^+ is the electronic hole. The MACE process was finished by removing the Ag particles from the silicon surface by HNO_3. Very sharp and deep structures were needed to reach sufficiently low reflectance. In this study, the texturization of the silicon wafers consisted of two steps. The wafers were firstly etched in alkaline solution consisting of 20 g of potassium hydroxide (KOH), 50 mL of isopropyl alcohol (IPA), and 1 L of deionized water at a temperature of 80 °C for 40 min to form randomly distributed pyramids in a micrometer scale on the silicon wafer surface. The size of the pyramids is not uniform, but generally, the base width and height of the pyramids are a few microns with an angle of about 54°. The wafer thickness was reduced to 170 μm. The wafers were then etched by a mixture of 0.6 M HF and 0.03 M $AgNO_3$ solutions at 40 °C for 1 to 9 min to produce nanostructures on the

pyramids. Figure 1d–f shows the schematic of the two-step texturization process. Shorter structures were able to significantly reduce the reflectance as compared to the conventional MACE process. After the MACE etching process, the wafers were cleaned by a standard Radio Corporation of America process, followed by a dip in HF for 1 min. For the passivation of the silicon wafers, an aluminum oxide (Al_2O_3) layer was deposited using a spatial ALD system (model AL_2O_3, Henghau Enterprise Co., Ltd., Taiwan) with trimethylaluminum (TMA) and water as the precursors. The gap between the ALD injector and movable substrate was 60 μm. The temperatures of the TMA and H_2O bubblers were 17.5 °C and 27 °C, respectively. The pipe temperature was 40 °C, which was higher than the bubblers temperature to avoid condensation. The substrate temperature was 150 °C. An inert gas N_2 was used as a curtain to isolate TMA and H_2O over the substrate. The growth per cycle of the Al_2O_3 was 0.17 nm/s, within the typical range reported in literature [19]. Afterwards, a silicon nitride (SiN_x) layer was deposited using radiofrequency inductively coupled plasma chemical vapor deposition (ICPCVD SI-500 D, SENTECH, Berlin, Germany) with a gas mixture of trimethylsilane and ammonia. The substrate temperature was 120 °C. The radiofrequency power was 1200 W. The deposition pressure was 5 mTorr. The ALD and ICPCVD processing parameters can also be found elsewhere [20]. For the characterization, the morphologies of the films were observed using a scanning electron microscope (SEM, JSM-7800F, JEOL, Tokyo, Japan). The reflectance of the wafers was measured using a UV-visible spectrometer (U-3900, Hitachi, Marunouchi, Japan). The injection-level dependent minority carrier lifetime of the wafers was measured using a lifetime tester (WCT-120, Sinton Instruments, Boulder, CO, USA). The cross-sectional images of the samples were obtained with a transmission electron microscope (TEM, JEM2100, JEOL, Tokyo, Japan) at 200 kV.

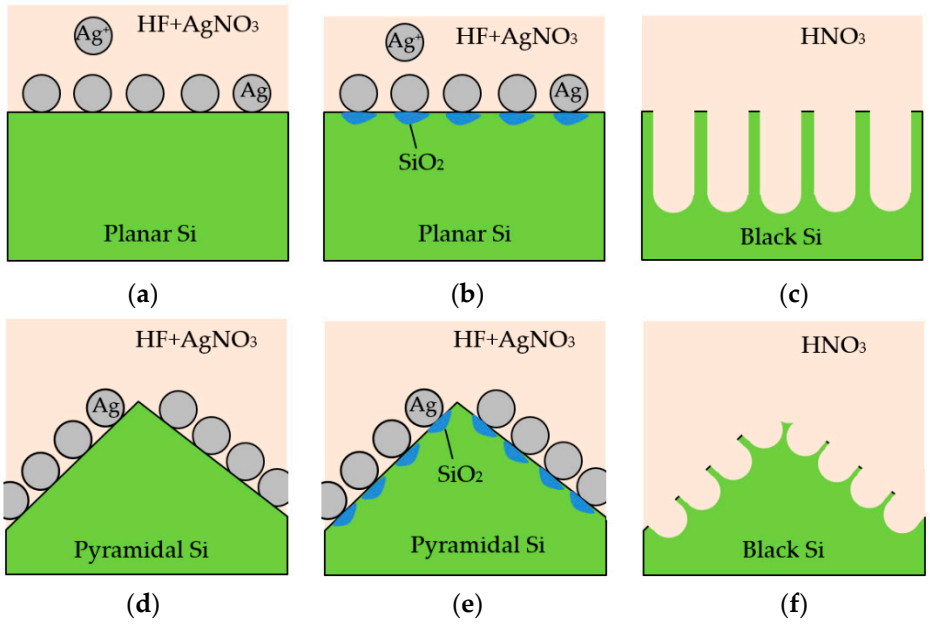

Figure 1. Schematic diagram of the metal-assisted chemical etching (MACE) process: (**a**) silver particles on the planar wafer; (**b**) local oxidation of Si on the surface; (**c**) sharp and deep needles formed after removing Ag particles by HNO_3; (**d**) silver particles on the pyramidal surface of an alkaline-etched silicon wafer; (**e**) silicon oxidation on the pyramidal surface; and (**f**) small-size needles formed on the pyramidal surface.

3. Results and Discussion

Two etching processes were applied to wafers for the surface texturing, which were alkaline etching to form randomly-distributed pyramids at a micrometer scale and MACE to further form needle-like structures in nanoscale. The etching time of the MACE process was varied. Figure 2 shows the SEM images of the silicon wafers without and with different MACE times. The wafer without

MACE in turn means that only alkaline etching was performed, and thus, a typical micrometer-scale pyramidal structure is formed on the wafer surface as shown in Figure 2a. There is no any substructure observable on the pyramid surfaces. The morphologies of the wafers change when the MACE time increases. At a MACE time of 1 min (Figure 2b), the wafer surface shows many shallow cavities, evidencing the removal of the silicon. The MACE time of 3 min produces pronounced needles on the pyramid surfaces as shown in Figure 2c. The size of the needles is not uniform, but the maximum height of the needles is roughly estimated to be 270 nm. Further increasing the MACE time remarkably enhances the development of the nanostructures, but with a height below 500 nm (Figure 2d–f). It is also noted that the some of the needles seem to connect to each other. In literature, the black silicon structures are mostly made by starting with a planar/polished wafer. Needles with a height at a micrometer level are needed in order to have sufficiently low reflectance [21,22]. Crystalline silicon solar cells usually have a shallow p–n junction with a junction depth of a few hundred nanometers from the front surface [23–25]. If the size of the nanostructures of the black silicon is larger than the junction depth, then the emitter diffusion process needs to be performed after the MACE process to avoid destroying the p–n junction. However, diffusion on such a silicon wafer with sharp needles is difficult. The nanostructure size in this study is not beyond the junction depth, and therefore, a standard diffusion process can be performed, followed by the MACE process.

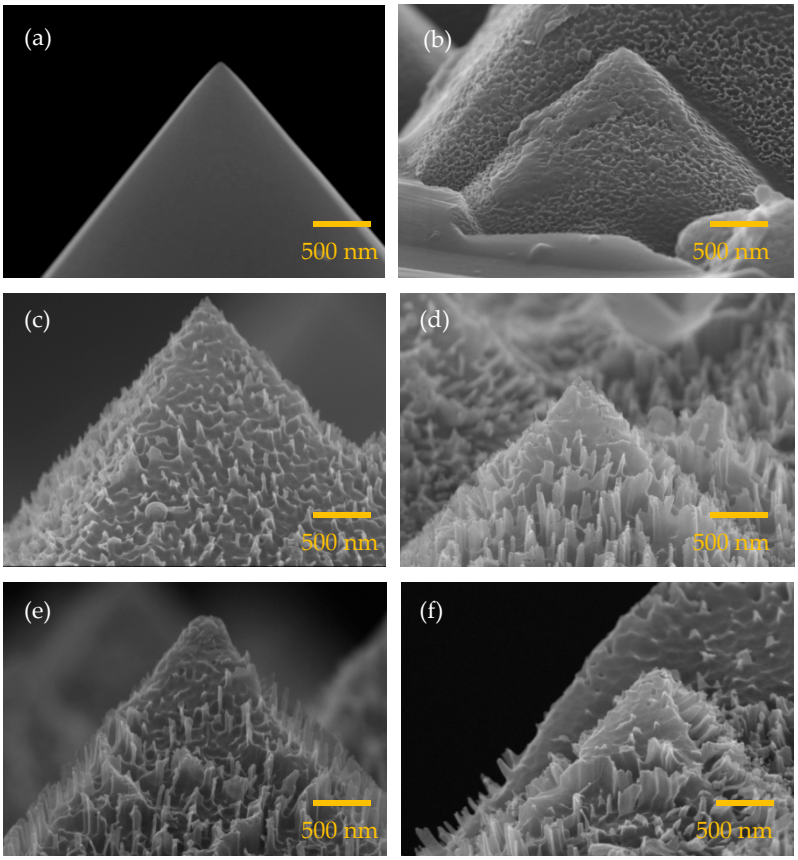

Figure 2. Scanning electron microscope (SEM) images for the alkaline-etched silicon wafers with the metal-assisted chemical etching (MACE) process for (**a**) 0, (**b**) 1, (**c**) 3, (**d**) 5, (**e**) 7, and (**f**) 9 min.

The reflectance spectra over 400–1000 nm of the alkaline-etched silicon wafers with different MACE time are shown in Figure 3a. The reflectance of the original wafer (with alkaline etching but without the MACE process) is in the range between 10–30%, similar to the wafer with a MACE time of 1 min. The wafers with MACE times of 3–9 min have a nearly identical reflectance in the short-wavelength region (400–550 nm), while the reflectance at the mid- to long-wavelengths (600–1000 nm) decreases with the MACE time. This result clearly evidences that the nanostructures of the wafers can reduce the

reflectance in the whole investigated wavelengths as compared to the wafer with the pyramidal surface. The average reflectance of the wafers is shown in Figure 3b. The values of the average reflectance of the wafers without MACE and with MACE time of 1 min are around 13%, a typical value for a wafer with a pyramidal surface. The average reflectance drops to 6.3% at a MACE time of 3 min. This reduction results from the presence of the needle-like structures. The wafers without and with a MACE time of 1 min show a silver-grey color, while the wafer with a MACE time of 3 min has a dark grey or nearly black color. The average reflectance further reduces from 6.3% to 4.6% when the MACE time increases from 3 to 9 min. Further increasing the etching time (not shown here) leads to slight or negligible reduction in average reflectance. This saturation behavior can be associated with the reduced concentration of HF in the etching solution. During the MACE process, the HF plays the role of removing silicon oxide. The amount of HF is consumed, and the removal released in the solution further decreases the concentration of HF. The etching process is thus expected to slow down and eventually stop. The MACE process performed on pyramidal surfaces of silicon wafers can achieve both low reflection and a small structure size.

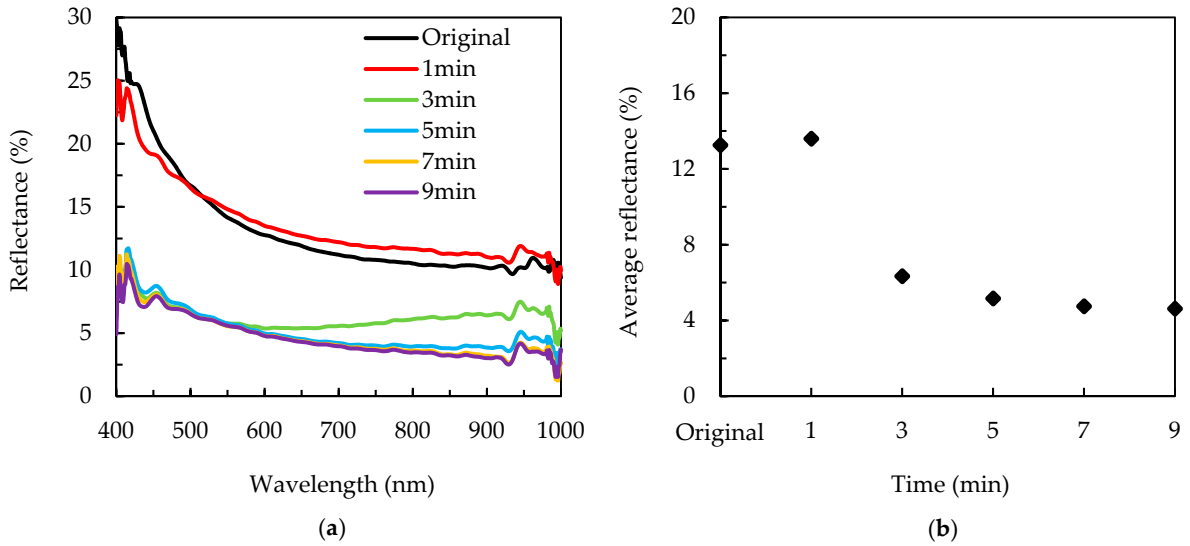

Figure 3. (**a**) Reflectance spectra and (**b**) average reflectance for the alkaline-etched silicon wafers with a different MACE time. The label "Original" refers to the sample with alkaline etching but without the MACE process.

Figure 4a shows the injection-level dependent minority carrier lifetime of the wafers with a different MACE time. The lifetime values at the injection level of 3×10^{15} cm^{-3} are shown in Figure 4b for comparison. Five samples were prepared for each MACE time, and the average values and error bars are indicated. It can be seen that the minority carrier lifetime of the original wafers (i.e., before MACE etching) already fluctuates from 7.8 to 11.4 µs with an average of 8.6 µs, and this could cause the variation of the lifetime of the wafers after the MACE process. However, the lifetime fluctuation of the original wafers is small, and thus, the impact is obvious for very low carrier lifetime values. For the passivated wafers with high carrier lifetime values, the impact is insignificant. The wafers with MACE times of 1–9 min show the minority carrier lifetime values in a range of 4–8.2 µs. All the wafers with MACE show a slight decrease in minority carrier lifetime. It has been demonstrated that the minority carrier lifetime decreases by increasing the front surface area [26,27]. The MACE processes lead to dangling bonds and dislocations that also result in a severe Shockley–Read–Hall recombination [18]. The small size of the developed nanostructures in the present study is helpful for mitigating the adverse effect.

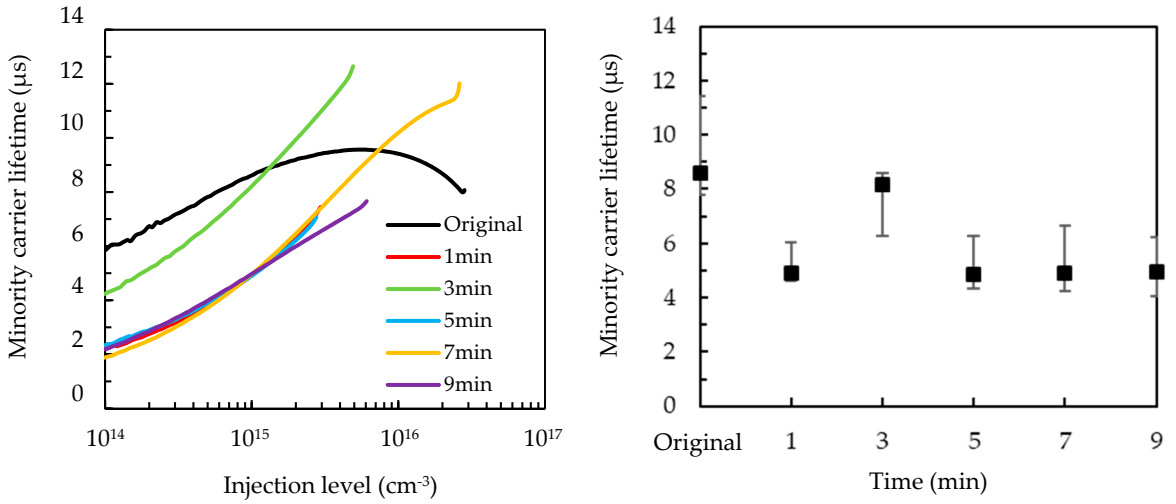

(**a**) (**b**)

Figure 4. (**a**) Injection-level dependent minority carrier lifetime; and (**b**) average minority carrier lifetime at the injection level of 3×10^{15} cm^{-3} for the alkaline-etched silicon wafers with a different MACE time.

It is required to further lower the reflectance and passivate the wafers. A stacked layer of SiN_x/Al_2O_3 is a good choice for use as antireflective layer and passivation layer [28,29]. Figure 5 shows the SEM images of the passivated wafers with a different MACE time. The thicknesses of the SiN_x and Al_2O_3 are respectively selected to be 90 and 15 nm. The insets of the figures are the close-up views. For the wafers without the MACE process, it can be seen that the passivation layer is smoothly covered on the wafer surface. A relatively rigid surface morphology can be observed for a MACE time of 1 min. The wafer with a MACE time of 3 min shows some rounded structures on the wafer surface, which is different to the needle-like structures before the deposition of the passivation layer. This change in the morphology indicates a low conformity of the passivation layer deposition. The rounded structures are more pronounced at MACE times of 5 and 7 min. At a MACE of 9 min, the wafer has needle-like structures, similar to the morphology before the passivation layer deposition. It is assumed that the passivation layer may either be conformally or hardly deposited. As the height of the nanostructures developed by the MACE process at 9 min is the largest, the passivation layer is more reasonable to be hardly deposited on the wafer rather than a conformal deposition.

To investigate the passivation quality, the injection-level dependent minority carrier lifetime values of the wafers after passivation are shown in Figure 6a, and the lifetime values at the injection level of 3×10^{15} cm^{-3} are shown in Figure 6b. The chemical passivation and field-effect passivation provided by the SiN_x/Al_2O_3 stacked layer reduce the surface recombination rate and increase the minority carrier lifetime as compared to the samples without the passivation layer. The original wafer (without the MACE process) has the highest lifetime value of around 250 μs, corresponding to a surface recombination rate of 34 cm/s. The original wafer has pyramids without sharp needles, and therefore, the passivation layer covers the surface well. As the MACE time increases from 1 to 9 min, the wafer lifetime decreases from 227.3 to 97.6 μs, and the surface recombination rate increases from 37.4 to 87.1 cm/s. This indicates that the passivation layer is not fully deposited on the wafers, especially for those connected needle structures. The SiN_x/Al_2O_3 films can hardly cover the boundaries or sidewalls of two narrow-spaced needles, leaving the dangling bonds unpassivated. Nevertheless, the currently standard c-Si solar cells use SiN_x single layer as the passivation layer of the front surface of the wafers, and the surface recombination rate is mostly in the level of 10^2 cm/s [30,31]. The low surface recombination rates for the samples in this study demonstrate a high surface passivation quality because of the ALD Al_2O_3 layer.

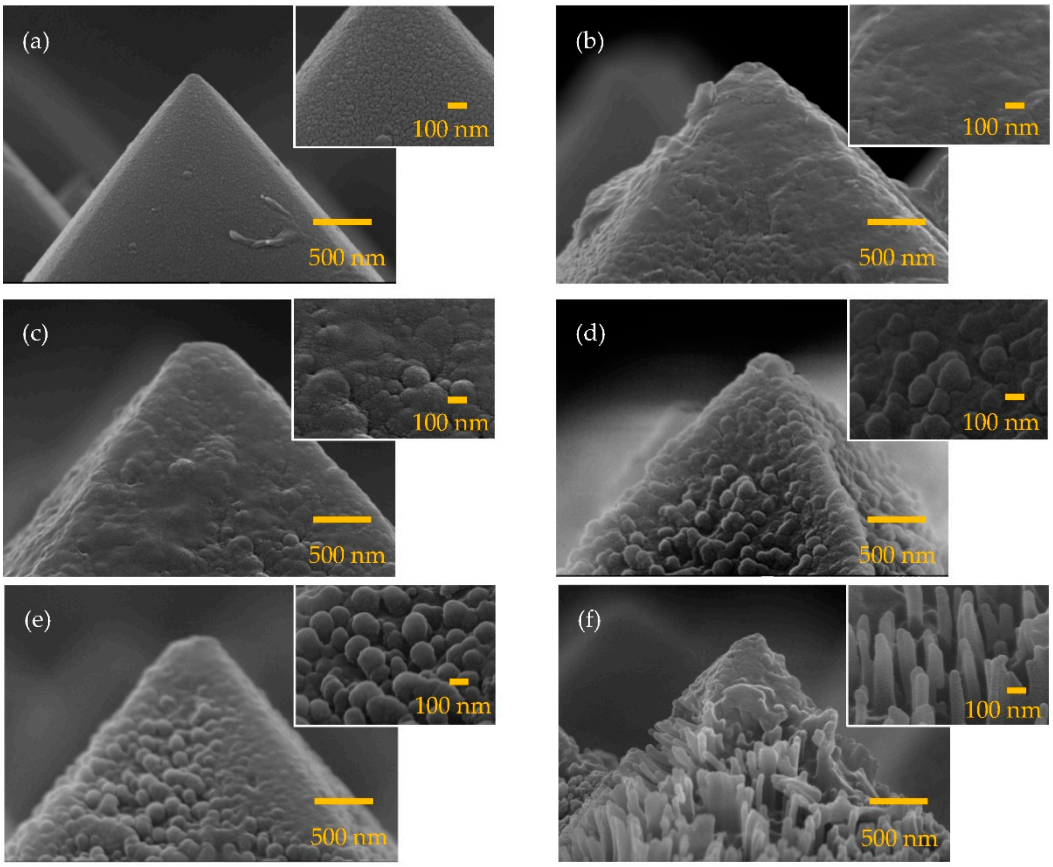

Figure 5. SEM images of the SiN_x/Al_2O_3-passivated wafers with MACE times of (**a**) 0; (**b**) 1; (**c**) 3; (**d**) 5; (**e**) 7; and (**f**) 9 min. The insets are a close-up view of the wafer surfaces.

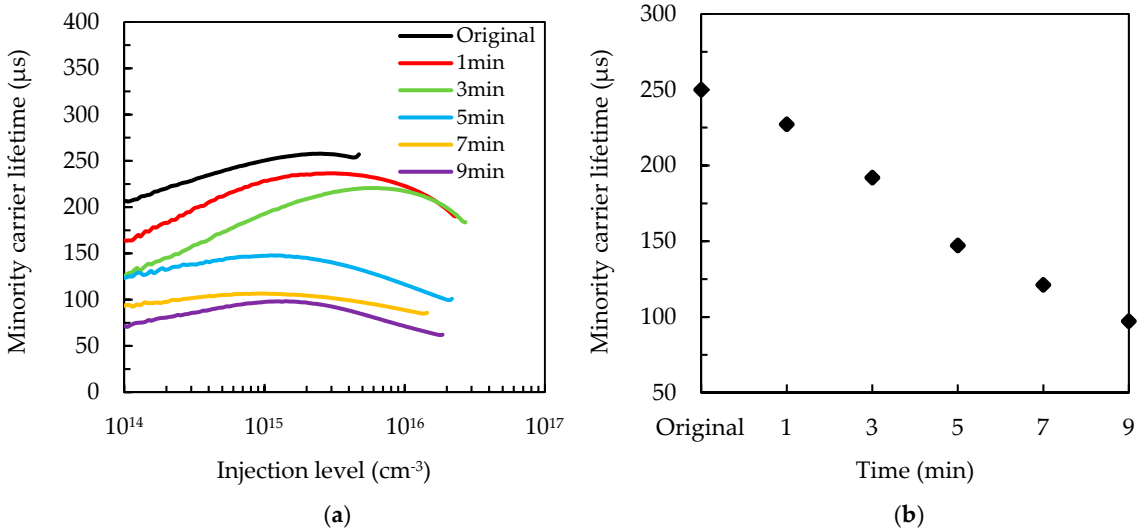

Figure 6. (**a**) Injection-level dependent minority carrier lifetime, and (**b**) average minority carrier lifetime at the injection level of 3×10^{15} cm^{-3} for the SiN_x/Al_2O_3-passivated silicon wafers with a different MACE time. The labeled "Original" refers to the passivated wafer with only alkaline etching but without the MACE process.

The reflectance spectra of the passivated wafers with different MACE times are shown in Figure 7a. The wafers without the MACE process and with a MACE time of 1 min show the curves with a single minimum reflectance. From the SEM image (Figure 2b), the 1 min MACE etching does not produce needle structures, while it creates shallow cavities and smoothens the tips and edges of the

pyramids. This is a possible reason for the higher reflectance of the 1 min MACE etched sample with the SiN_x/Al_2O_3 stack compared to the others. This is a typical shape of a reflectance spectrum curve for an antireflective layer deposited on silicon. The wafers with MACE times of 3–9 min exhibit a low reflectance in broad wavelengths. The average reflectance values are shown in Figure 7b. For the alkaline-etched wafer with SiN_x/Al_2O_3, the reflectance is 4.7%. A minimal reflectance of 3.6% is reached at a MACE time of 3 min. The reflectance increases with further increase of the MACE time. The increase in reflectance for long MACE times is presumably due to the poor coverage of the SiN_x/Al_2O_3 layers. The wafer with a MACE time of 9 min has a reflectance of 4.9%, nearly same as before the deposition of SiN_x/Al_2O_3 layers. This also confirms that the antireflection layer is hardly coated on the wafer. It is known that ALD is able to provide a very high conformity deposition, and thus, the coating problem should arise from the PECVD SiN_x deposition. Other research groups also reported that the PECVD has difficulties of gap filling or depositing void-free films on high aspect ratio structures [32,33].

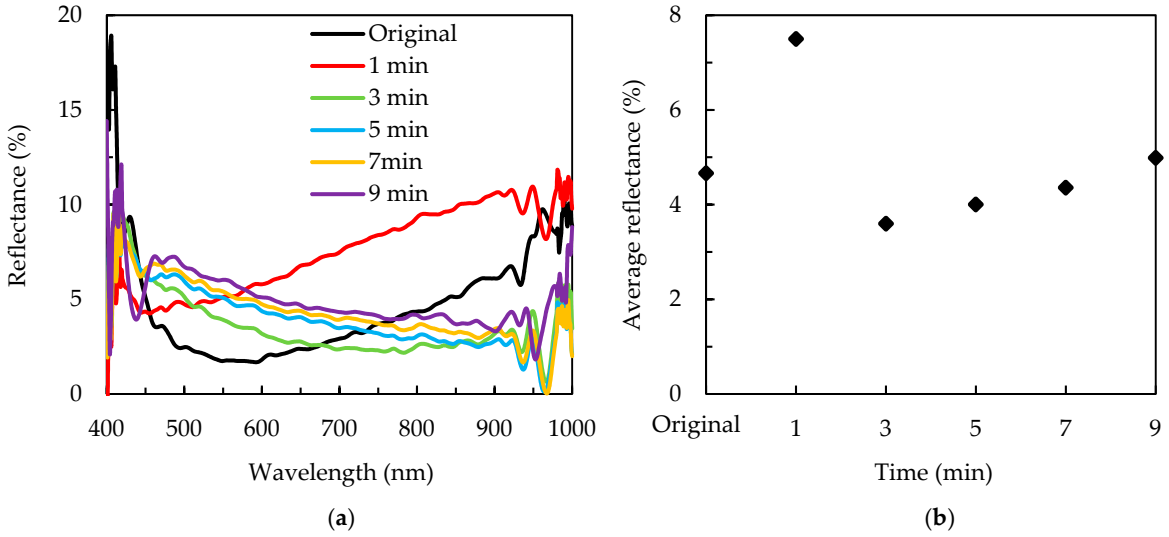

Figure 7. (**a**) Reflectance spectra, and (**b**) average reflectance for the SiN_x/Al_2O_3 passivated silicon wafers with a different MACE time.

The thickness of the SiN_x is varied from 54 to 90 nm to further optimize the reflectance for the 3 min MACE etched sample. The thickness of the Al_2O_3 is kept to 15 nm. Figure 8a shows the reflectance spectra for the wafers with different SiN_x thickness. The labeled "Original" refers to the pyramidal wafer with the 90 nm SiN_x/15 nm Al_2O_3 stacked layer. The average reflectance is shown in Figure 8b. The refractive indices of the SiN_x and Al_2O_3 are 1.8 and 1.7, respectively. For conventional silicon crystalline solar cells, the SiN_x single antireflective layer should have an optimal thickness of 80–90 nm according to the quarter-wavelength formula to achieve a reflectance minimum at 550–600 nm. The average reflectance over 400–1000 nm of the 90 nm SiN_x-covered pyramidal silicon wafers is around 4% (not shown). In order to have high passivation, the pyramidal wafer is covered with not only 90 nm SiN_x but 15 nm Al_2O_3, and this in turn means that the total thickness of the antireflective layer becomes larger, resulting in a slight increase of reflectance to 4.6%. By adjusting SiN_x thickness, the reflectance of the 3 min MACE etched wafer decreases to its minimum of 1.4% at the SiN_x thickness of 72 nm. The total thickness of SiN_x/Al_2O_3 is 87 nm.

Figure 9 shows the cross-sectional images of the 72 nm SiN_x/15 nm Al_2O_3-passivated pyramidal silicon wafers with a MACE time of 3 min. The nanostructures with heights of 200–300 nm can be seen in Figure 9a. Close-up views are taken for some regions labeled as b–d. In region b (Figure 9b), the SiN_x/Al_2O_3 is covered on the top of the pyramid. The SiN_x is the thickest on the top, and the thickness decreases obviously at the valley. The Al_2O_3 shows a uniform thickness when covering on the wafer. It is noted that for the nanostructures on the right-hand side, the Al_2O_3 can still be well

deposited, whereas the SiN_x only covers on the top of the nanostructure. Thus, there is an absence of SiN_x at two nanostructures, as appearing in white-grey color in the image. Similar results can be observed in Figure 9c,d. At the sidewall of the pyramidal surface, both of the Al_2O_3 and SiN_x can be well deposited, but the SiN_x cannot fill the gap between the nanostructures. These empty spaces indicate that ALD passivation is necessary for black silicon; otherwise, the traditional PECVD films are hardly covered on the surfaces.

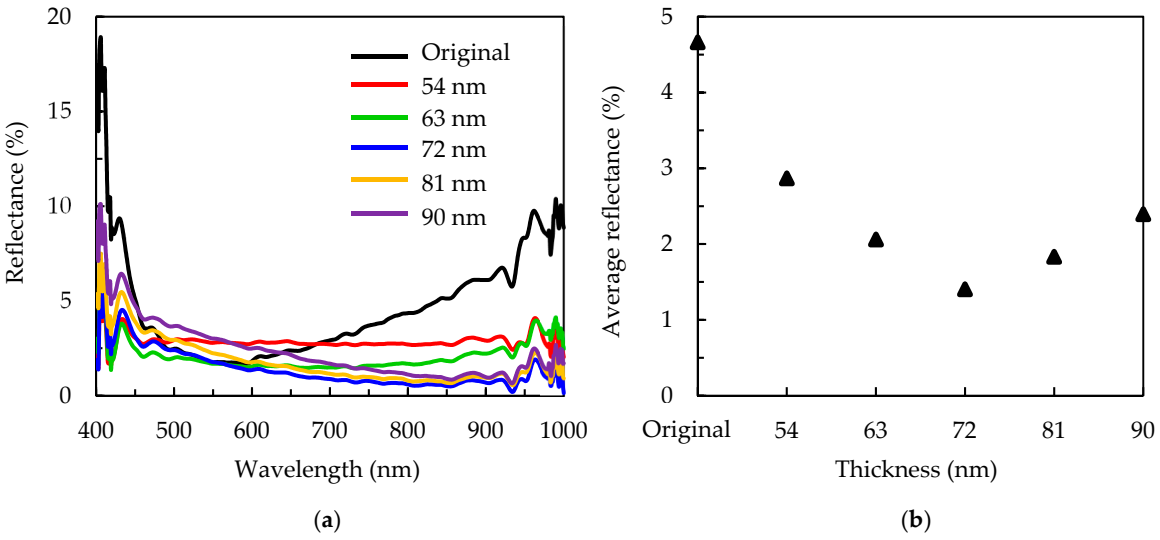

Figure 8. (**a**) Reflectance spectra, and (**b**) average reflectance for the 3 min MACE-treated silicon wafers covered with different SiN_x thickness. The labeled "Original" refers to the pyramidal silicon wafer (without the MACE process) with the 90 nm SiN_x/15 nm Al_2O_3 stacked layer.

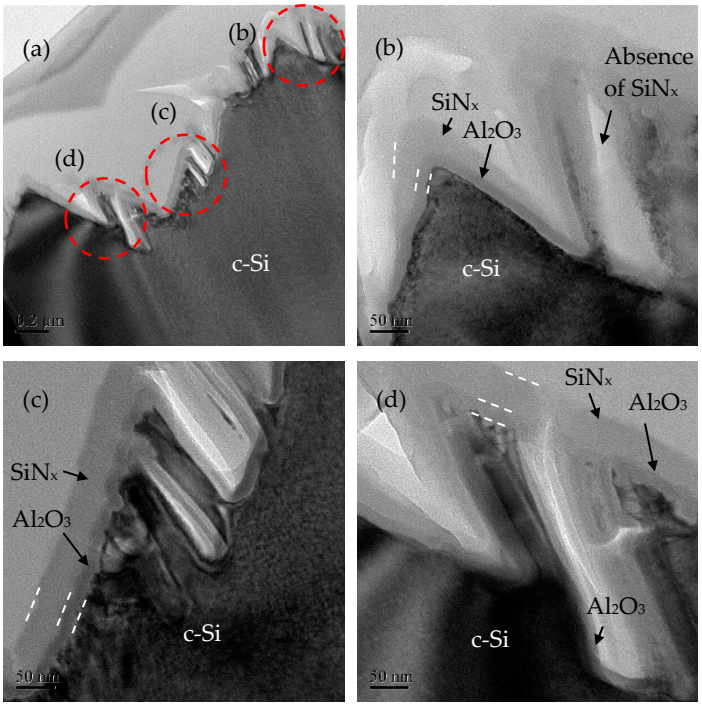

Figure 9. (**a**) Cross-sectional transmission electron microscope (TEM) images for black silicon with a MACE time of 3 min and SiN_x/Al_2O_3 passivation layers. The red circles are different locations in the black silicon wafer, and (**b**–**d**) are their close-up views.

The black silicon with a MACE time of 3 min and 72 nm SiN_x/15 nm Al_2O_3 passivation demonstrates a reflectance of 1.4% and a surface recombination rate of 43.6 cm/s. Currently, conventional crystalline silicon mainstream PV products have a pyramidal front surface with a SiN_x single layer as an antireflective layer and passivation layer. The average reflectance is around 4%, and the surface recombination rate is at a level of 10^2 cm/s. These values could be used for estimating the gain in short-circuit current density (J_{sc}) and open-circuit voltage (V_{oc}) in the device level, as given by [34,35]:

$$J_{sc} = \int [1 - R(\lambda)] IQE(\lambda) S(\lambda) d\lambda \quad (4)$$

$$V_{oc} = \frac{kT}{q} \ln\left(\frac{J_{sc}}{J_{0b} + J_{0e}} + 1\right) \quad (5)$$

where λ is the wavelength, R is the reflectance, IQE is the internal quantum efficiency, S is the solar spectrum, kT/q is the thermal voltage, J_{0b} is the base dark current, and J_{0e} is the emitter dark current. For simplification by assuming that the MACE process only influences the surface of the wafers and does not affect IQE, the variation of J_{sc} can be evaluated by R. Equation (4) gives that the J_{sc} for the black silicon can increase by 2.6% compared to that for the traditional c-Si. For the variation of V_{oc}, it is determined by J_{0e} as the black silicon nanostructures are designed on the light-receiving side (emitter side). J_{0e} is given by [36]:

$$J_{0e} = \frac{q n_i^2 W}{2} \frac{1}{N_B + \Delta n} \frac{1}{\tau_{suf}} \quad (6)$$

where q is the electron charge, n_i is the intrinsic carrier concentration, W is the wafer thickness, N_B is the bulk doping concentration, Δn is the excess carrier concentration (3×10^{15} cm^{-3}), and τ_{suf} is the lifetime associated with the surface recombination. By assuming the infinite bulk lifetime, τ_{suf} is equal to the measured effective minority carrier lifetime. The calculated J_{0e} is about 53 fA/cm^2 for black silicon and 113 fA/cm^2 for the conventional c-Si solar cell. It is considered that only the surface property is affected, while the others are not influenced by the MACE process. Thus, from Equations (5) and (6), the V_{oc} of the black silicon increases by 2% compared to that of the conventional cells. Another way to evaluate the open-circuit voltage is the one-sun implied V_{oc} obtained from the WCT-120 lifetime measurement. Table 1 lists the implied V_{oc} for different nanostructures passivated by the SiN_x/Al_2O_3 stack. The labeled "Reference" corresponds to the SiN_x single layer-passivated pyramidal wafer. The implied V_{oc} of the 3 min MACE etched wafer is about 2.1% higher than that of the reference sample, and the gain is in agreement with that evaluated by using J_{0e}. Overall, as the solar cell conversion efficiency is the multiplication of V_{oc}, J_{sc} and fill factor, the black silicon proposed in this work is helpful for increasing the c-Si solar cell efficiency.

Table 1. One-sun implied V_{oc} of the SiN_x/Al_2O_3-passivated silicon wafers with different MACE time. The labeled "Reference" corresponds to the SiN_x single layer-passivated pyramidal wafer.

MACE Time (min)	Implied V_{oc} (mV)
Reference	676
1	692
3	690
5	688
7	684
9	679

4. Conclusions

Needle-like nanostructures were prepared on pyramidal surfaces of c-Si using MACE processes. The reflectance can greatly reduce to below 5% when the height of the needle-structures is below 500 nm, typically smaller than the junction depth of c-Si solar cells. A SiN_x/Al_2O_3 stacked layer is covered on the black silicon surface as an antireflective and passivation layer. The ALD Al_2O_3 film is found to be conformally deposited on the black silicon, while the PECVD SiN_x film shows a poorer coverage or is even hardly coated between two needle-like structures. The optimum MACE time is 3 min, and the passivated wafer exhibits a nanostructure height of less than 300 nm, the lowest reflectance of 1.4% and a low surface recombination rate of 43.6 cm/s. Compared to the currently standard c-Si solar cells with a reflectance of about 4% and a front surface recombination rate at 10^2 cm/s level, the black silicon technique proposed in this work is helpful for improving the solar cell conversion efficiency.

Author Contributions: Conceptualization, C.-H.H. and S.-Y.L.; formal analysis, C.-H.H., S.-M.L., X.-Y.Z., S.Z., S.-Y.C., and W.-Z.Z.; investigation, C.-H.H., S.-M.L., X.-Y.Z., Y.-S.C., and Y.-H.H.; supervision, S.-Y.L.; writing—original draft preparation, C.-H.H.; writing—review and editing, C.-H.H. and S.-Y.L.; funding acquisition, X.-Y.Z.

Funding: This work was sponsored by the science and technology project of Xiamen (No. 3502Z20183054) and the Science and Technology Program of the Educational Office of Fujian Province (No. JT180432).

Conflicts of Interest: The authors declare no conflict of interest.

References

1. Zhao, J.; Green, M.A. Optimized antireflection coatings for high-efficiency silicon solar cells. *IEEE Trans. Electron Devices* **1991**, *38*, 1925–1934. [CrossRef]
2. Otto, M.; Algasinger, M.; Branz, H.; Gesemann, B.; Gimpel, T.; Füchsel, K.; Käsebier, T.; Kontermann, S.; Koynov, S.; Li, X.; et al. Black Silicon Photovoltaics. *Adv. Opt. Mater.* **2015**, *3*, 147–164. [CrossRef]
3. Liu, X.; Coxon, P.R.; Peters, M.; Hoex, B.; Cole, J.M.; Fray, D.J. Black silicon: Fabrication methods, properties and solar energy applications. *Energy Environ. Sci.* **2014**, *7*, 3223–3263. [CrossRef]
4. Wu, C.; Crouch, C.H.; Zhao, L.; Carey, J.E.; Younkin, R.; Levinson, J.A.; Mazur, E.; Farrell, R.M.; Gothoskar, P.; Karger, A. Near-unity below-band-gap absorption by microstructured silicon. *Appl. Phys. Lett.* **2001**, *78*, 1850–1852. [CrossRef]
5. Ma, L.L.; Zhou, Y.C.; Jiang, N.; Lu, X.; Shao, J.; Lu, W.; Ge, J.; Ding, X.M.; Hou, X.Y. Wide-band "black silicon" based on porous silicon. *Appl. Phys. Lett.* **2006**, *88*, 171907. [CrossRef]
6. Koynov, S.; Brandt, M.S.; Stutzmann, M. Black nonreflecting silicon surfaces for solar cells. *Appl. Phys. Lett.* **2006**, *88*, 203107. [CrossRef]
7. Nishioka, K.; Horita, S.; Ohdaira, K.; Matsumura, H. Antireflection subwavelength structure of silicon surface formed by wet process using catalysis of single nano-sized gold particle. *Sol. Energy Mater. Sol. Cells* **2008**, *92*, 919–922. [CrossRef]
8. Tsujino, K.; Matsumura, M.; Nishimoto, Y. Texturization of multicrystalline silicon wafers for solar cells by chemical treatment using metallic catalyst. *Sol. Energy Mater. Sol. Cells* **2006**, *90*, 100–110. [CrossRef]
9. Yoo, J.; Yu, G.; Yi, J. Black surface structures for crystalline silicon solar cells. *Mater. Sci. Eng. B* **2009**, *159–160*, 333–337. [CrossRef]
10. Nayak, B.K.; Iyengar, V.V.; Gupta, M.C. Efficient light trapping in silicon solar cells by ultrafast-laser-induced self-assembled micro/nano structures. *Prog. Photovolt. Res. Appl.* **2011**, *19*, 631–639. [CrossRef]
11. Liu, Y.; Lai, T.; Li, H.; Wang, Y.; Mei, Z.; Liang, H.; Li, Z.; Zhang, F.; Wang, W.; Kuznetsov, A.Y.; et al. Nanostructure Formation and Passivation of Large-Area Black Silicon for Solar Cell Applications. *Small* **2012**, *8*, 1392–1397. [CrossRef] [PubMed]
12. Srivastava, S.K.; Kumar, D.; Singh, P.K.; Kar, M.; Kumar, V.; Husain, M. Excellent antireflection properties of vertical silicon nanowire arrays. *Sol. Energy Mater. Sol. Cells* **2010**, *94*, 1506–1511. [CrossRef]
13. Koynov, S.; Brandt, M.S.; Stutzmann, M. Black multi-crystalline silicon solar cells. *Phys. Status Solidi RRL—Rapid Res. Lett.* **2007**, *1*, R53–R55. [CrossRef]

14. Srivastava, S.K.; Kumar, D.; Sharma, M.; Kumar, R.; Singh, P.K. Silver catalyzed nano-texturing of silicon surfaces for solar cell applications. *Sol. Energy Mater. Sol. Cells* **2012**, *100*, 33–38. [CrossRef]
15. Branz, H.M.; Yost, V.E.; Ward, S.; Jones, K.M.; To, B.; Stradins, P. Nanostructured black silicon and the optical reflectance of graded-density surfaces. *Appl. Phys. Lett.* **2009**, *94*, 231121. [CrossRef]
16. Stephens, R.B.; Cody, G.D. Optical reflectance and transmission of a textured surface. *Thin Solid Films* **1977**, *45*, 19–29. [CrossRef]
17. Christesen, J.D.; Zhang, X.; Pinion, C.W.; Celano, T.A.; Flynn, C.J.; Cahoon, J.F. Design Principles for Photovoltaic Devices Based on Si Nanowires with Axial or Radial p–n Junctions. *Nano Lett.* **2012**, *12*, 6024–6029. [CrossRef] [PubMed]
18. Oh, J.; Yuan, H.-C.; Branz, H.M. An 18.2%-efficient black-silicon solar cell achieved through control of carrier recombination in nanostructures. *Nat. Nanotechnol.* **2012**, *7*, 743–748. [CrossRef]
19. Ellinger, C.R.; Nelson, S.F. Selective Area Spatial Atomic Layer Deposition of ZnO, Al_2O_3, and Aluminum-Doped ZnO Using Poly(vinyl pyrrolidone). *Chem. Mater.* **2014**, *26*, 1514–1522. [CrossRef]
20. Hsu, C.H.; Cho, Y.S.; Wu, W.Y.; Lien, S.Y.; Zhang, X.Y.; Zhu, W.Z.; Zhang, S.; Chen, S.-Y. Enhanced Si Passivation and PERC Solar Cell Efficiency by Atomic Layer Deposited Aluminum Oxide with Two-step Post Annealing. *Nanoscale Res. Lett.* **2019**, *14*, 139. [CrossRef] [PubMed]
21. Ma, S.; Liu, S.; Xu, Q.; Xu, J.; Lu, R.; Liu, Y.; Zhong, Z. A theoretical study on the optical properties of black silicon. *AIP Adv.* **2018**, *8*, 035010. [CrossRef]
22. Repo, P.; Benick, J.; Vähänissi, V.; Schön, J.; von Gastrow, G.; Steinhauser, B.; Schubert, M.C.; Hermle, M.; Savin, H. N-type Black Silicon Solar Cells. *Energy Procedia* **2013**, *38*, 866–871. [CrossRef]
23. Shen, L.; Liang, Z.C.; Liu, C.F.; Long, T.J.; Wang, D.L. Optimization of oxidation processes to improve crystalline silicon solar cell emitters. *AIP Adv.* **2014**, *4*, 027127. [CrossRef]
24. Cheon, S.; Jeong, D.S.; Park, J.-K.; Kim, W.M.; Lee, T.S.; Lee, H.; Kim, I. Enhanced blue responses in nanostructured Si solar cells by shallow doping. *J. Phys. Appl. Phys.* **2018**, *51*, 125102. [CrossRef]
25. Lee, K.; Kim, S.; Kim, Y.; Park, C.; Balaji, N.; Han, C.; Choi, B.; Lee, J.; Dao, V.A.; Lee, Y.-J.; et al. Optimization of the Junction Profile Through Control of the Doping Heat Profile for Silicon Solar Cell Applications. *J. Nanosci. Nanotechnol.* **2017**, *17*, 3224–3228. [CrossRef]
26. Zhou, Z.-Q.; Hu, F.; Zhou, W.-J.; Chen, H.-Y.; Ma, L.; Zhang, C.; Lu, M. An Investigation on a Crystalline-Silicon Solar Cell with Black Silicon Layer at the Rear. *Nanoscale Res. Lett.* **2017**, *12*, 623. [CrossRef] [PubMed]
27. Shieh, J.; You, C.; Chiu, C.; Liu, J.; Shih, P. Black-Silicon on Micropillars with Minimal Surface Area Enlargement to Enhance the Performance of Silicon Solar Cells. *Nanoscale Res. Lett.* **2016**, *11*, 489. [CrossRef]
28. Allen, T.G.; Bullock, J.; Jeangros, Q.; Samundsett, C.; Wan, Y.; Cui, J.; Hessler-Wyser, A.; De Wolf, S.; Javey, A.; Cuevas, A. A Low Resistance Calcium/Reduced Titania Passivated Contact for High Efficiency Crystalline Silicon Solar Cells. *Adv. Energy Mater.* **2017**, *7*, 1602606. [CrossRef]
29. Tao, Y.; Upadhyaya, V.; Chen, C.-W.; Payne, A.; Chang, E.L.; Upadhyaya, A.; Rohatgi, A. Large area tunnel oxide passivated rear contact *n* -type Si solar cells with 21.2% efficiency: Large area tunnel oxide passivated rear contact *n* -type Si solar cells. *Prog. Photovolt. Res. Appl.* **2016**, *24*, 830–835. [CrossRef]
30. Min, B.; Muller, M.; Wagner, H.; Fischer, G.; Brendel, R.; Altermatt, P.P.; Neuhaus, H. A Roadmap Toward 24% Efficient PERC Solar Cells in Industrial Mass Production. *IEEE J. Photovolt.* **2017**, *7*, 1541–1550. [CrossRef]
31. Huang, H.; Lv, J.; Bao, Y.; Xuan, R.; Sun, S.; Sneck, S.; Li, S.; Modanese, C.; Savin, H.; Wang, A.; et al. 20.8% industrial PERC solar cell: ALD Al 2 O 3 rear surface passivation, efficiency loss mechanisms analysis and roadmap to 24%. *Sol. Energy Mater. Sol. Cells* **2017**, *161*, 14–30. [CrossRef]
32. Lu, T.-J.; Fanto, M.; Choi, H.; Thomas, P.; Steidle, J.; Mouradian, S.; Kong, W.; Zhu, D.; Moon, H.; Berggren, K.; et al. Aluminum nitride integrated photonics platform for the ultraviolet to visible spectrum. *Opt. Express* **2018**, *26*, 11147. [CrossRef] [PubMed]
33. Yang, H.; Chuwongin, S.; Qiang, Z.; Chen, L.; Pang, H.; Ma, Z.; Zhou, W. Resonance control of membrane reflectors with effective index engineering. *Appl. Phys. Lett.* **2009**, *95*, 023110. [CrossRef]
34. Takei, K. (Ed.) *Flexible and Stretchable Medical Devices*; Wiley-VCH: Weinheim, Germany, 2018; ISBN 978-3-527-80485-6.

35. Roy, J.N.; Bose, D.N. *Photovoltaic Science and Technology*, 1st ed.; Cambridge University Press: Cambridge, UK, 2017; ISBN 978-1-108-41524-8.
36. Lu, G.; Zheng, F.; Wang, J.; Shen, W. Thin Al_2O_3 passivated boron emitter of n-type bifacial c-Si solar cells with industrial process. *Prog. Photovolt. Res. Appl.* **2017**, *25*, 280–290. [CrossRef]

© 2019 by the authors. Licensee MDPI, Basel, Switzerland. This article is an open access article distributed under the terms and conditions of the Creative Commons Attribution (CC BY) license (http://creativecommons.org/licenses/by/4.0/).